Chinese Chemical Letters 35 (2024) 110030

Contents lists available at ScienceDirect

Chinese Chemical Letters

journal homepage: www.elsevier.com/locate/cclet

High sensitivity artificial synapses using printed high-transmittance ITO fibers for neuromorphic computing

Shangda Qu[a,b], Yiming Yuan[a,b], Xu Ye[a,b], Wentao Xu[a,b,*]

[a] Institute of Photoelectronic Thin Film Devices and Technology, Key Laboratory of Photoelectronic Thin Film Devices and Technology of Tianjin, College of Electronic Information and Optical Engineering, Engineering Research Center of Thin Film Photoelectronic Technology of Ministry of Education, Smart Sensing Interdisciplinary Science Center, Nankai University, Tianjin 300350, China
[b] Shenzhen Research Institute of Nankai University, Shenzhen 518000, China

ARTICLE INFO

Article history:
Received 9 April 2024
Revised 17 May 2024
Accepted 19 May 2024
Available online 20 May 2024

Keywords:
Solid polymer electrolyte
ITO fibers
Artificial synapses
Synaptic plasticity
Neuromorphic computing

ABSTRACT

Artificial synapses are essential building blocks for neuromorphic electronics. Here, solid polymer electrolyte-gated artificial synapses (EGASs) were fabricated using ITO fibers as channels, which possess an ultra-high sensitivity of 5 mV and a long-term memory time exceeding 3 min. Notably, digitally printed ITO-fiber arrays exhibit an ultra-high transmittance of approximately 99.67%. Biological synaptic plasticity, such as excitatory postsynaptic current, paired-pulse facilitation, spike frequency-dependent plasticity, and synaptic potentiation and depression, were successfully mimicked using the EGASs. Based on the synaptic properties of the EGASs, an artificial neural network was constructed to perform supervised learning using the Fashion-MNIST dataset, achieving high pattern recognition rate (82.39%) due to the linear and symmetric synaptic plasticity. This work provides insights into high-sensitivity artificial synapses for future neuromorphic computing.

In the era of data deluge, conventional computing systems that operate on the von Neumann architecture, which is characterized by a clear division between storage and processing components, face substantial challenges [1-3]. In contrast, the human brain utilizes a vast number of neurons ($\sim 10^{11}$) connected by synapses ($\sim 10^{15}$) to perform distributed, parallel, and event-driven computations, conferring benefits in terms of fault tolerance, computing speed, and energy efficiency [4-6]. Especially, synapses can perform functions for memory and learning by tuning their connection strength, known as synaptic plasticity [7]. Consequently, the development of neuromorphic computing, which emulates the human brain's computational approach by integrating memory and processing in a single unit, is of great significance in overcoming the von Neumann bottleneck.

Artificial synapses that can emulate functions of biological synapses are the basic units for neuromorphic computing [8-10]. Various types of artificial synapses have been prepared to emulate synaptic plasticity including two-terminal memristors and three-terminal synaptic transistors [11-17]. Three-terminal devices possess advantages in that they can receive and read stimuli concurrently and have multiple gates to deal with spatiotemporal information [18,19]. However, three-terminal artificial synapses still need improvements in the linearity and symmetry of conductance change, sensitivity, and memory time to meet the requirements of the hardware implementation of neural networks.

In this work, we fabricated solid polymer electrolyte-gated artificial synapses (EGASs) using ITO fibers as channels, achieving an ultra-high sensitivity (5 mV) and a long-term memory time (>3 min). The EGASs can emulate various biological synaptic functions and are suitable for associative learning. Furthermore, an artificial neural network was established utilizing the synaptic characteristics of EGASs for supervised learning with the Fashion-MNIST dataset. Thanks to the linear and symmetric synaptic plasticity, the network exhibited a pattern recognition rate of up to 82.39%. Additionally, directionally ordered ITO fibers fabricated using electrohydrodynamic printing exhibited an ultra-high transmittance of approximately 99.67%, which holds potential for applications in transparent electronics. This work is of great significance for both transparent and neuromorphic electronics.

ITO fibers were prepared using an electrohydrodynamic printer. The ink was fabricated by dissolving stannous chloride dihydrate ($SnCl_2{\cdot}2H_2O$), indium nitrate trihydrate ($In(NO_3)_3{\cdot}xH_2O$), and poly(vinylpyrrolidone) (PVP) in *N*,*N*-dimethylformamide (DMF) and stirring the mixture at 50 °C for 6 h. The printed parameters were as follows: printing voltage of 1.1 kV, injection rate of 40 nL/min,

* Corresponding author.
E-mail address: wentao@nankai.edu.cn (W. Xu).

https://doi.org/10.1016/j.cclet.2024.110030
1001-8417/

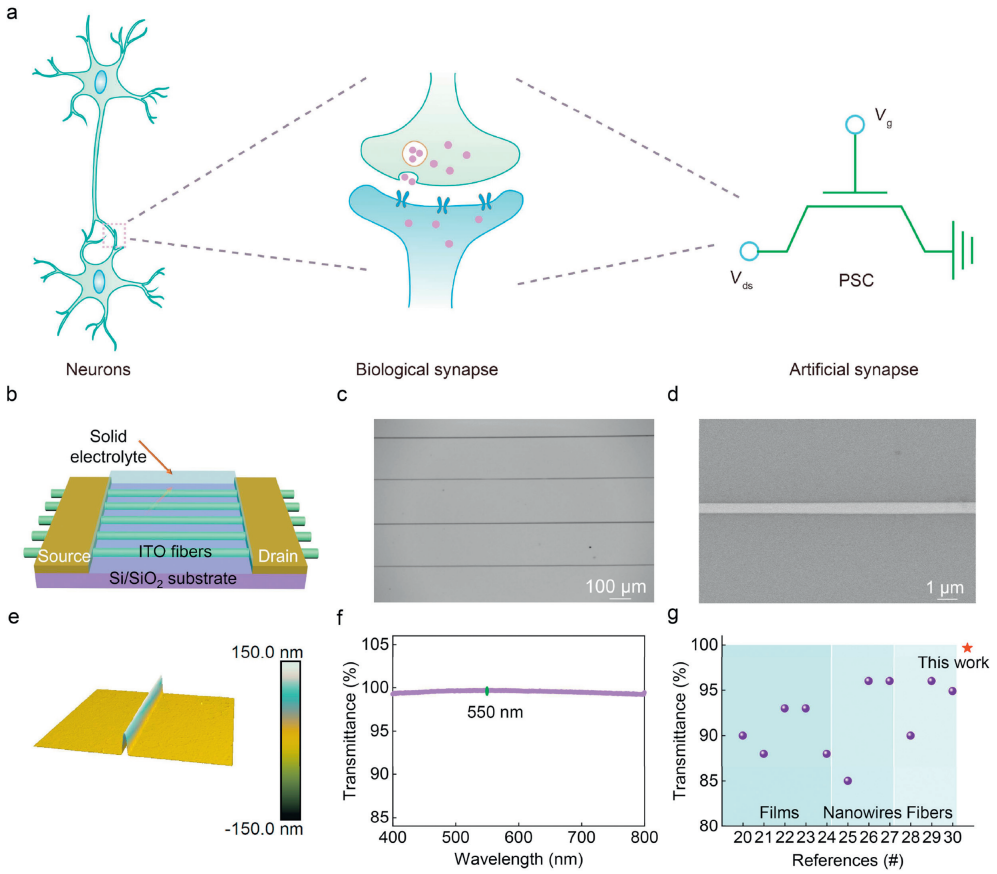

Fig. 1. (a) Schematic of the biological synapse and three-terminal artificial synapse. (b) Structure of the EGAS. (c) OM image of ITO fibers arrays. (d) SEM image of a single ITO fiber. (e) AFM image of a single ITO fiber. (f) Visible range transmittance of the ITO fibers. (g) Transmittance comparison between our ITO fibers and previously reported ITO materials with various morphologies.

substrate speed of 1 m/s, and a nozzle-to-collector distance of 3 mm. Subsequently, the printed samples were calcined to obtain these ITO fibers under 500 °C for 120 min.

For the fabrication of the EGASs, gold electrodes (~80 nm) were thermally deposited onto the prepared ITO fibers. The solid polymer electrolyte was prepared by mixing lithium perchlorate ($LiClO_4$, 0.2 g) with poly(ethylene oxide) (PEO, 1.6 g) powders in acetonitrile (30 mL). This mixture was drop-coated onto the surface of the ITO fibers and then annealed in a nitrogen (N_2) atmosphere at 90 °C for 20 min to form the gate dielectric layer. The input terminal was employed a metal probe to apply presynaptic stimuli.

The details of material and device characterization methods employed in this study are as follows. A scanning electron microscope (SEM) (Apreo S, Thermo Scientific) and an optical microscope (OM) (DM2700M, Leica) were employed to observe the morphology of ITO fibers. An atomic force microscope (AFM) (Dimension Icon, Bruker) was employed to measure the height of ITO fibers. The optical transmission spectrum was obtained with the aid of UV-vis-NIR spectrophotometer (Cary 5000, Agilent). All electrical measurements of the artificial synapses were conducted inside a glove box filled with N_2 at room temperature, using a Keithley 4200A semiconductor parameter analyzer with the assistance of a probe station.

To emulate biological synapses, three-terminal artificial synapses were designed (Fig. 1a). These artificial synapses utilized directionally ordered ITO fibers as channels and a solid polymer electrolyte as the gate dielectric layer (Fig. 1b). The molecular structure of PEO is shown in Fig. S1 (Supporting information). The spacing between adjacent fibers was ~200 μm (Fig. 1c and Fig. S2 in Supporting information). A single fiber showed a diameter of ~470 nm as observed in the SEM image (Fig. 1d). The three-dimensional shape of ITO fibers with a height of ~130 nm was visualized using an AFM image (Fig. 1e and Fig. S3 in Supporting information). Notably, the ITO fibers exhibited ultra-high transmittance of ~99.67% at 550 nm (Fig. 1f). The transmittance of our ITO fibers exhibited a significant advantage over previously reported ITO materials with different morphologies (Fig. 1g and Table S1 in Supporting information), demonstrating their potential for applications in the field of transparent electronics [20-30].

The transfer characteristics of the EGAS, ranging from −3 V to 3 V under a drain voltage (V_d) of 0.05 V, exhibited a significant hysteresis loop (Fig. 2a), demonstrating that the carriers in the ITO fibers were effectively modulated by the mobile ions in the solid polymer electrolyte. The output characteristics of the EGAS was shown in Fig. S4 (Supporting information). Upon application of a single presynaptic spike (2 V, 50 ms) to the gate under $V_d = 0.05$ V, the cations in the solid polymer electrolyte migrated to the interface between the electrolyte and the ITO fibers, leading to the creation of an electric double layer. Consequently, electrons in ITO fibers accumulated on their surface due to the electrostatic coupling effect, inducing the formation of an excitatory postsynaptic current (EPSC). After removal of the presynaptic spike, the cations within the solid polymer electrolyte returned to a random distribution, leading to a progressive decrease in the EPSC towards a value close to the baseline (Fig. 2b).

Paired-pulse facilitation (PPF) offers advantages in spatiotemporal information processing as a type of short-term plasticity (STP) [31,32]. Upon application of a pair of presynaptic spikes (2 V, 50 ms) with a time interval (Δt) of 100 ms to the gate, the ΔEPSC

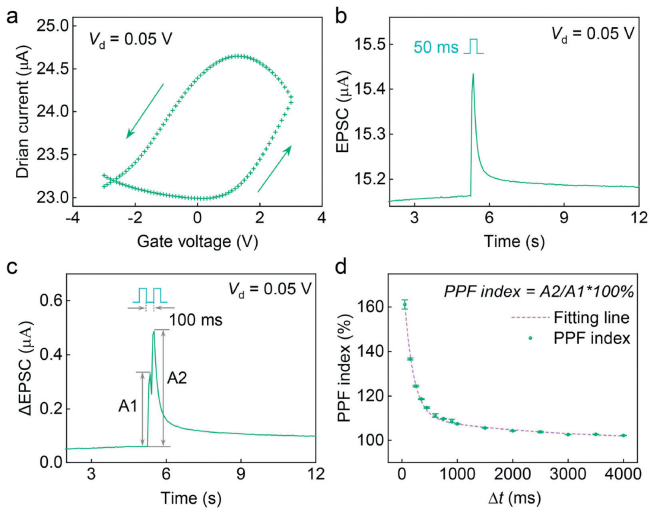

Fig. 2. (a) Transfer characteristics of the EGAS at $V_d = 0.05$ V. (b) EPSC of the EGAS triggered by a single presynaptic spike. (c) ΔEPSC of the EGAS triggered by a pair of presynaptic spikes. (d) PPF index as a function of time interval between spikes for the EGAS.

peak evoked by the second spike (A2) was significantly larger than that evoked by the first spike (A1) (Fig. 2c). The second spike arrived before all of the cations driven by the first spike had returned to a random distribution, thus the second ΔEPSC peak was larger. Furthermore, applying many pairs of spikes with different Δt (from 50 ms to 4000 ms) to the gate, the EGAS maintained PPF characteristics (Fig. S5 in Supporting information). Here, the PPF index, defined as $(A2/A1) \times 100\%$, was shown as mean values and standard deviations, which progressively decreased as Δt increased due to the increased time available for the cations to return to a random distribution (Fig. 2d). The PPF index decay was fitted using a double exponential equation with rapid decay and slow decay components (Eq. 1) [33]:

$$\text{PPF indx} = C_1 \times \exp\left(-\frac{\Delta t}{\tau_1}\right) + C_2 \times \exp\left(-\frac{\Delta t}{\tau_2}\right) + 100\% \qquad (1)$$

where C_n and τ_n are the initial facilitation magnitudes and time constants for the rapid (n = 1) and slow (n = 2) decay processes, respectively. The fitted τ_1 and τ_2 values are approximately 162.2 and 2408.5 ms, respectively.

Biological synapses can process dynamic real-time information through spike frequency-dependent plasticity (SFDP) [34,35]. SFDP of the EGAS was quantified by applying ten consecutive presynaptic spikes (2 V, 50 ms) at various frequencies (from 0.5 Hz to 10 Hz) at $V_d = 0.05$ V. ΔEPSC increased with increasing spike frequency (Fig. 3a). SFDP index was defined as $(Bn/B1) \times 100\%$, where Bn and B1 are the ΔEPSC peaks triggered by the n^{th} and the 1^{st} spikes, respectively. The SFDP index increased as the spike frequency increased (Fig. 3c), which can be attributed to the reduced time for cations to return to a random distribution. These results indicate that the EGAS may have potential application in image processing as a high-pass filter.

Spike number-dependent plasticity (SNDP) is a learning mechanism where successive external stimuli may adjust the quantity of neurotransmitters released at a synapse, thereby modulating the synaptic weight [36]. When presynaptic spikes (2 V, 50 ms) with different numbers ranging from 1 to 10 were applied to the EGAS, the ΔEPSC peaks increased progressively (Fig. 3b). The SNDP index was defined as $(Cn/C1) \times 100\%$, where Cn and C1 represent the ΔEPSC peaks triggered by presynaptic spikes with quantities of n and 1, respectively. The SNDP index monotonically increased with the increasing spike number (Fig. 3d), which is a result of the accumulation of cations at the interface between ITO fibers and the solid polymer electrolyte.

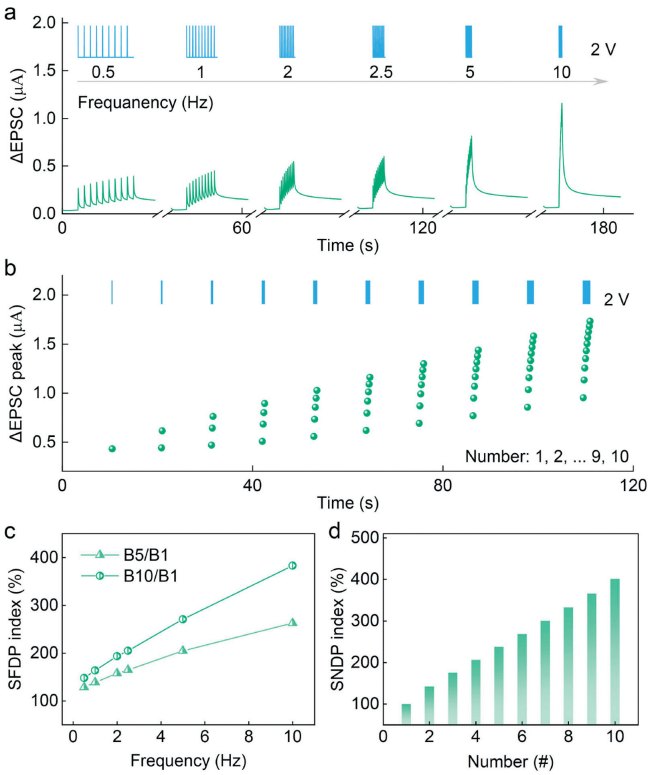

Fig. 3. (a) ΔEPSC of the EGAS triggered by consecutive presynaptic spikes with different frequencies. (b) ΔEPSC peak of the EGAS triggered by presynaptic spikes with different numbers. (c) SFDP index *versus* spike frequencies. (d) SNDP index *versus* spike numbers.

Long-term plasticity (LTP) forms the basis for memory formation [37]. The EGAS transitioned from STP to LTP by increasing the amplitude and duration of presynaptic spikes. Under $V_d = 0.05$ V, the ΔEPSC monotonically increased with increasing spike amplitudes from 1 V to 5 V (Fig. 4a), demonstrating spike voltage-dependent plasticity. As the durations of presynaptic spikes (2 V) increased from 50 ms to 550 ms at $V_d = 0.05$ V, both ΔEPSC and the ΔEPSC peak also monotonically increased (Fig. 4b and Fig. S6 in Supporting information), illustrating spike duration-dependent plasticity. These phenomena are attributed to the enhanced electrostatic coupling effect under strong stimuli.

Moreover, the memory time and sensitivity of the EGAS were characterized. The decay time of the ΔEPSC evoked by 50 consecutive presynaptic spikes (2 V, 50 ms) under $V_d = 0.05$ V exceeded 3 min, indicating its favorable LTP (Fig. 4c). The EGAS exhibited ultra-high sensitivity, responsive to a 5 mV presynaptic spike at $V_d = 0.05$ V (Fig. 4d).

Due to the long memory time, the EGAS can be used to simulate classical Pavlovian associative learning (Fig. 4e). Two distinct patterns are employed to represent the "bell" and "bone" stimuli, with a threshold set at 1 μA. The "bell" pattern, initiated by ten spikes (1 V, 50 ms), acting as a neutral stimulus, initially fails to induce salivation. Conversely, the "bone" pattern, initiated by ten larger spikes (2 V, 50 ms), representing a conditioned stimulus, effectively triggers salivation. During training, the patterns are presented alternately, allowing the subject to associate the "bell" with the "bone", leading to salivation. Post-training, the "bell" pattern alone is sufficient to elicit a salivation response, indicating successful simulation of Pavlovian associative learning.

To demonstrate the potential application of the EGAS in neuromorphic computing, an artificial neural network with three layers

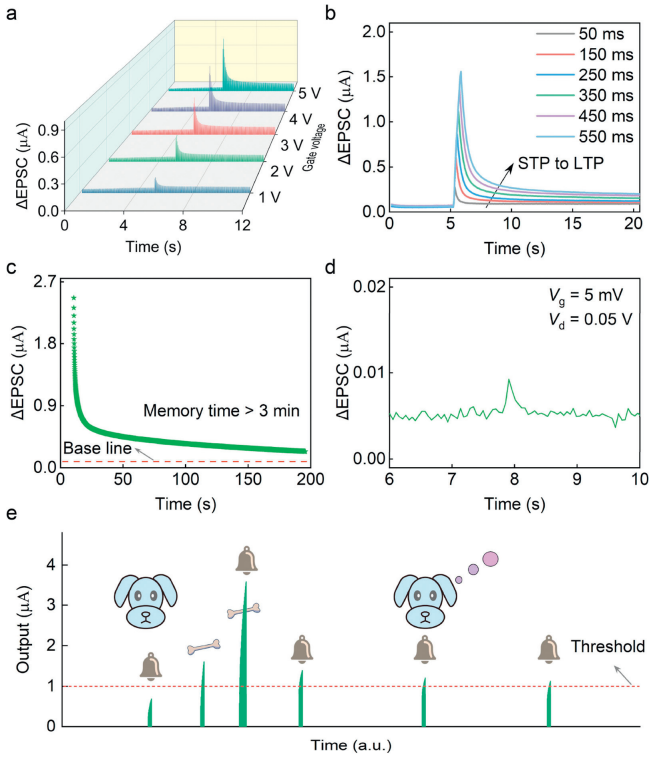

Fig. 4. (a) ΔEPSC of the EGAS triggered by presynaptic spikes with different amplitudes. (b) ΔEPSC of the EGAS triggered by presynaptic spikes with different durations. (c) Memory time of the EGAS. (d) ΔEPSC of the EGAS triggered by presynaptic spikes of 5 mV. (e) Pavlovian learning behavior realized using the EGAS.

was constructed to perform system-level training and recognition tasks using the Fashion Modified National Institute of Standards and Technology database (Fashion-MNIST) dataset [38,39]. The designed artificial neural network features a structure that includes an input layer, a hidden layer, and an output layer (Fig. 5a). Each input vector corresponds to a pixel of the Fashion-MNIST image that connects with an input neuron. The input vectors are multiplied by the synaptic weights that utilize the stochastic gradient descent algorithm to update based on the difference between the output value and the labeled value. Finally, these results are transformed by a softmax activation function to obtain the output vectors.

Successive cycles of potentiation (30 spikes of 2 V) and depression (30 spikes of −1.5 V) at $V_d = 0.05$ V for the EGAS exhibited good stability (Fig. 5b). The EGAS showed linear and symmetric synaptic potentiation/depression (Fig. 5c). The non-linearity parameter α was extracted using the following equation (Eq. 2) [40,41]:

$$G = \begin{cases} \left(\left(G_{LRS}^{\alpha} - G_{HRS}^{\alpha}\right) \times w + G_{HRS}^{\alpha}\right)^{\frac{1}{\alpha}} & if\ \alpha \neq 0, \\ G_{HRS} \times \left(\frac{G_{LRS}}{G_{HRS}}\right)^{w} & if\ \alpha = 0. \end{cases} \quad (2)$$

where G is the conductance change, G_{LRS} and G_{HRS} are the conductance in the low resistance state (LRS) and high resistance state (HRS), respectively; w is an internal variable ranging from 0 to 1; α is the non-linearity parameter that controls potentiation (α_p) or depression (α_d) characteristics. The linearity increases as α approaches 1, and the degree of symmetry is higher with a smaller difference between α_p and α_d [41]. For the EGAS, α_p and α_d were fitted as 0.90 and 0.83, respectively, indicating its linear and symmetric synaptic plasticity. Based on the above synaptic properties, the traits of the images are recognized accurately through enough

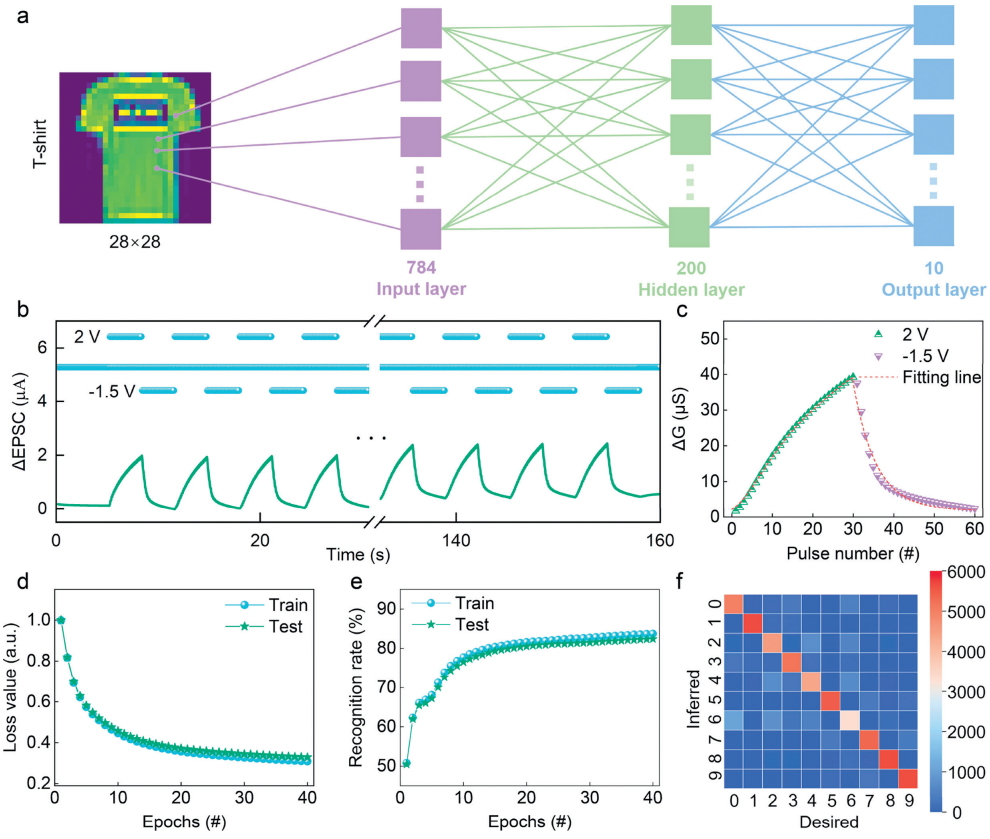

Fig. 5. (a) Structure of the artificial neural network. (b) Successive cycles potentiation (2 V) and depression (−1.5 V) of the EGAS. (c) Potentiation and depression of the EGAS *versus* spike numbers. (d) Loss value *versus* training epochs. (e) Recognition rate *versus* training epochs. (f) Confusion matrix for pattern recognition after training epoch 40.

training. As the training epochs gradually increased, the loss value decreased and the recognition rate increased monotonically (Figs. 5d and e, Fig. S7 in Supporting information). The recognition rate reached an impressive 82.39% after 40 training epochs (Figs. 5e and f). These results demonstrated our devices have applications in neuromorphic computing.

In summary, we fabricated solid polymer electrolyte-gated artificial synapses (EGASs) with an ultra-high sensitivity (5 mV) and a long-term memory time (>3 min). Directionally ordered ITO fibers, fabricated using electrohydrodynamic printing, were employed as the channels of the EGASs, achieving an ultra-high transmittance of approximately 99.67%, which holds potential for applications in transparent electronics. The EGASs can emulate various synaptic plasticity and are suitable for associative learning. Furthermore, an artificial neural network was established according to the synaptic characteristics of the EGASs to conduct supervised learning using the Fashion-MNIST dataset, achieving a high pattern recognition rate of ~82.39% due to the linear and symmetric synaptic plasticity. This work offers a novel contribution to the field of neuromorphic devices, holding significant relevance for the advancement of transparent electronics and neuromorphic computing.

Declaration competing of interests

The authors declare that they have no known competing financial interests or personal relationships that could have appeared to influence the work reported in this paper.

CRediT authorship contribution statement

Shangda Qu: Writing – original draft, Visualization, Investigation, Formal analysis, Data curation, Conceptualization. **Yiming Yuan:** Software, Formal analysis, Data curation. **Xu Ye:** Visualization, Investigation. **Wentao Xu:** Writing – review & editing, Supervision, Project administration, Funding acquisition, Conceptualization.

Acknowledgments

This work was supported by the National Science Fund for Distinguished Young Scholars of China (No. T2125005), the National Key R&D Program of China (Nos. 2022YFE0198200, 2022YFA1204500, 2022YFA1204504), the Shenzhen Science and Technology Project (No. JCYJ20210324121002008), the Natural Science Foundation of Tianjin (Nos. 22JCYBJC01290, 23JCQNJC01440), the Key Project of Nature Science Foundation of Tianjin (No. 22JCZDJC00120), and the Fundamental Research Funds for the Central Universities, Nankai University (Nos. BEG124901, BEG124401).

Supplementary materials

Supplementary material associated with this article can be found, in the online version, at doi:10.1016/j.cclet.2024.110030.

References

[1] K. Roy, A. Jaiswal, P. Panda, Nature 575 (2019) 607–617.
[2] X. Liu, S. Dai, W. Zhao, et al., Adv. Mater. 36 (2024) 2312473.
[3] D. Marković, A. Mizrahi, D. Querlioz, et al., Nat. Rev. Phys. 2 (2020) 499–510.
[4] Y. Kim, A. Chortos, W. Xu, et al., Science 360 (2018) 998–1003.
[5] J.Q. Yang, R. Wang, Y. Ren, et al., Adv. Mater. 32 (2020) e2003610.
[6] J. Yu, Y. Wang, S. Qin, et al., Mater. Today 60 (2022) 158–182.
[7] Y. Park, M.K. Kim, J.S. Lee, J. Mater. Chem. C 9 (2021) 5396–5402.
[8] X. Luo, J. Ming, J. Gao, et al., Front. Neurosci. 16 (2022) 1016026.
[9] Y. Gao, J. Zhang, D. Liu, et al., Chin. Chem. Lett. 35 (2024) 108582.
[10] R. Yu, E. Li, X. Wu, et al., ACS Appl. Mater. Interfaces 12 (2020) 15446–15455.
[11] Y. Park, J.S. Lee, J. Phys. Chem. Lett. 13 (2022) 5638–5647.
[12] A. Chanthbouala, V. Garcia, R.O. Cherifi, et al., Nat. Mater. 11 (2012) 860–864.
[13] K.E. Harabi, T. Hirtzlin, C. Turck, et al., Nat. Electron. 6 (2022) 52–63.
[14] Y. Liu, Y. Wang, X. Li, et al., Chin. Chem. Lett. 34 (2023) 107842.
[15] S. Wang, X. Shi, J. Gong, et al., Nano Lett. 24 (2024) 3204–3212.
[16] S. Qu, J. Liu, J. Hu, et al., Adv. Fiber Mater. 6 (2024) 401–413.
[17] D.H. Ho, D.G. Roe, Y.Y. Choi, et al., Sci. Adv. 8 (2022) eabn1838.
[18] H. Han, H. Yu, H. Wei, et al., Small 15 (2019) 1900695.
[19] S. Dai, X. Liu, Y. Liu, et al., Adv. Mater. 35 (2023) 2300329.
[20] A.H. Ali, Z. Hassan, A. Shuhaimi, Appl. Surf. Sci. 443 (2018) 544–547.
[21] J.L. Chiang, S.W. Li, B.K. Yadlapalli, et al., Vacuum 186 (2021) 110046.
[22] M.J. Alam, D.C. Cameron, Thin Solid Films 377-378 (2000) 455–459.
[23] M. Gulen, G. Yildirim, S. Bal, et al., J. Mater. Sci. Mater. El. 24 (2012) 467–474.
[24] Y. Ren, P. Liu, R. Liu, et al., J. Alloy. Compd. 893 (2022) 162304.
[25] Q. Wan, E.N. Dattoli, W.Y. Fung, et al., Nano Lett. 6 (2006) 2909–2915.
[26] Y.Y. Kee, S.S. Tan, T.K. Yong, et al., Nanotechnology 23 (2012) 025706.
[27] Q. Li, Z. Tian, Y. Zhang, et al., Sci. Rep. 9 (2019) 4983.
[28] M.M. Munir, F. Iskandar, K.M. Yun, et al., Nanotechnology 19 (2008) 145603.
[29] H. Wu, L. Hu, T. Carney, et al., J. Am. Chem. Soc. 133 (2011) 27–29.
[30] S. Yoon, H. Kim, E.S. Shin, et al., ACS Appl. Mater. Interfaces 9 (2017) 34305–34313.
[31] S. Qu, L. Sun, S. Zhang, et al., Nat. Commun. 14 (2023) 7181.
[32] Y. Xu, G. Zhang, W. Liu, et al., SmartMat 4 (2023) e1162.
[33] J. Gao, Y. Zheng, W. Yu, et al., SmartMat 2 (2021) 88–98.
[34] X. Wang, H. Yang, E. Li, et al., Small 19 (2023) 2205395.
[35] J. Chen, Z. Zhou, B.J. Kim, et al., Nat. Nanotechnol. 18 (2023) 882–888.
[36] W. Huang, P. Hang, Y. Wang, et al., Nano Energy 73 (2020) 104790.
[37] L. Guo, Q. Wan, C. Wan, et al., IEEE Electr. Device Lett. 34 (2013) 1581–1583.
[38] H. Wei, G. Yao, Y. Ni, et al., Adv. Funct. Mater. 33 (2023) 2304000.
[39] L. Jiang, L. Yang, Y. Yuan, et al., ACS Mater. Lett. 6 (2024) 1606–1615.
[40] J.W. Jang, S. Park, G.W. Burr, et al., IEEE Electr. Device Lett. 36 (2015) 457–459.
[41] M.E. Pereira, J. Deuermeier, P. Freitas, et al., APL Mater. 10 (2022) 011113.